bioRxiv preprint doi: https://doi.org/10.1101/084152; this version posted May 11, 2017. The copyright holder for this preprint (which was not certified by peer review) is the author/funder, who has granted bioRxiv a license to display the preprint in perpetuity. It is made available under aCC-BY-NC-ND 4.0 International license.

Conditioning by subthreshold synaptic input changes the characteristic firing pattern of CA3 hippocampal neurons

Saray Soldado-Magraner[1*☯], Federico Brandalise[2,3,☯], Suraj Honnuraiah[1], Michael Pfeiffer[1], Urs Gerber[2], Rodney Douglas[1],

1 Institute of Neuroinformatics, University of Zurich and ETH Zurich, Switzerland
2 Brain Research Institute, University of Zurich, Switzerland
3 Center for Learning and Memory, University of Texas at Austin, EEUU

☯These authors contributed equally to this work.
* ssaray@ini.uzh.ch

Abstract

Neurons are typically classified according to their intrinsic firing patterns and distinctive morphological features. However, our experiments in the CA3 field of rat hippocampus in vitro revealed that discharge patterns change significantly following a short period of low frequency subthreshold stimulation of the neuron's afferents. This effect could be reproduced by intrasomatic current pulses and was blocked by kinase inhibitors. Cluster analysis of the firing patterns before and after conditioning revealed systematic transitions towards adapting and intrinsic burst behaviours, irrespective of the initial pattern exhibited by the cell. Using a conductance-based model, we demonstrate that the observed transitions can be mediated by recruitment of calcium and M-type potassium conductances. We conclude that CA3 neurons adapt their conductance profile to the statistics of ongoing activity in their embedding circuits, making their intrinsic firing pattern not a constant signature, but rather the reflection of long-term circuit activity.

Author summary

Various anatomical types of neuron generate characteristic patterns of action potential discharge in response to intra-somatic injections of step currents. Together with the cell's morphology and molecular markers, these patterns have been used to classify neuronal phenotypes. However, in this study we show that in the case of hippocampal CA3 neurons this discharge behavior is not as characteristic as generally assumed. Instead, the dynamics of a neuron's supra-threshold output behavior may change significantly over a time scale of many minutes in response to sub-threshold input. Although this input is too small to evoke a spike response, the neurons nevertheless appear to adjust their membrane conductances by a mechanism that involves phosphorylation. Future suprathreshold step inputs will then elicit a different characteristic pattern of spikes. These results suggest that instead of being relatively static input-output devices, CA3 neurons modify their fundamental configuration of operation according to long-term statistics of the small on-going signals that they receive from other members of their embedding circuit.

bioRxiv preprint doi: https://doi.org/10.1101/084152; this version posted May 11, 2017. The copyright holder for this preprint (which was not certified by peer review) is the author/funder, who has granted bioRxiv a license to display the preprint in perpetuity. It is made available under aCC-BY-NC-ND 4.0 International license.

Introduction

It is widely accepted that the diversity of morphological, molecular, and electrophysiological properties exhibited by neurons of the neocortex and hippocampus reflects functionally distinct classes of cells [1–7]. In particular, neurons have been classified electrophysiologically according to the pattern of their action potential discharge in response to applied intra-somatic step currents. Many studies have reported that excitatory and different types of inhibitory neurons, identified by morphology and molecular markers, exhibit distinct firing patterns [6, 8–13]. These responses may be for example: adapting, accelerating, bursting, or fast spiking. With rare exceptions [14], the patterns are assumed to be a sufficiently stable property of a neuron to be used as a basis for phenotypic classification [6, 15–17]. A prominent view is that genetic factors determine both the morphology and the distinct firing patterns of individual neurons [15]. However, there are substantial reasons to doubt that discharge patterns are indeed static properties of neurons. The discharge response of a neuron depends on the distribution and activations of the membrane conductances that it expresses [6, 18]. This distribution is subject to homeostatic control including up- or down-regulation of conductances in response to the neuron's own activity [19–21]. For example, somatogastric ganglion (STG) neurons of the lobster change their firing patterns in response to network isolation by changing the balance between inward and outward currents [19]. Furthermore, neurons have conserved molecular pathways that link network activity to the recruitment of genes and signaling factors implicated in neural excitability [22, 23], and activity-dependent maturation is indeed necessary for the emergence of the whole spectrum of electrical types [24, 25]. In final agreement with this hypothesis, a recent study shows for the first time that the electrical properties of different types of basket cells can be interchanged in response to neural activity [26]. These lines of evidence suggest that the firing pattern is not a static characteristic of the cell, but rather the consequence of adaptive mechanisms that adjust the behavior of the neuron in response to the patterns of activity in its embedding network. We have explored this hypothesis using whole-cell recordings from neurons in the CA3 region of rat hippocampus in organotypic cultures. The discharge patterns of neurons in response to constant current injection were characterized before and after a conditioning phase of periodic subthreshold synaptic stimulation. It was found that pre-conditioned cells could indeed be classified according to the type of their discharge pattern. However, conditioning by subthreshold synaptic input elicited significant changes in the behavior of most of the neurons examined, requiring substantial re-classification of their type. This effect was reproduced when conditioning the cells via intra-somatic current pulses. The effect was blocked by adding protein kinase A (PKA) and protein kinase C (PKC) inhibitors to the recording pipette, suggesting that changes are mediated at the single cell level via phosphorylation. We used a conductance-based single compartment neuron model to explore which changes in the neuronal conductance profile could underlay the observed changes in discharge pattern. We found that the results can be explained by a recruitment of voltage dependent calcium and M-type potassium ion channels. We conclude that CA3 neurons can indeed adapt their output patterns in response to circuit activity by by possibly tuning key conductances.

bioRxiv preprint doi: https://doi.org/10.1101/084152; this version posted May 11, 2017. The copyright holder for this preprint (which was not certified by peer review) is the author/funder, who has granted bioRxiv a license to display the preprint in perpetuity. It is made available under aCC-BY-NC-ND 4.0 International license.

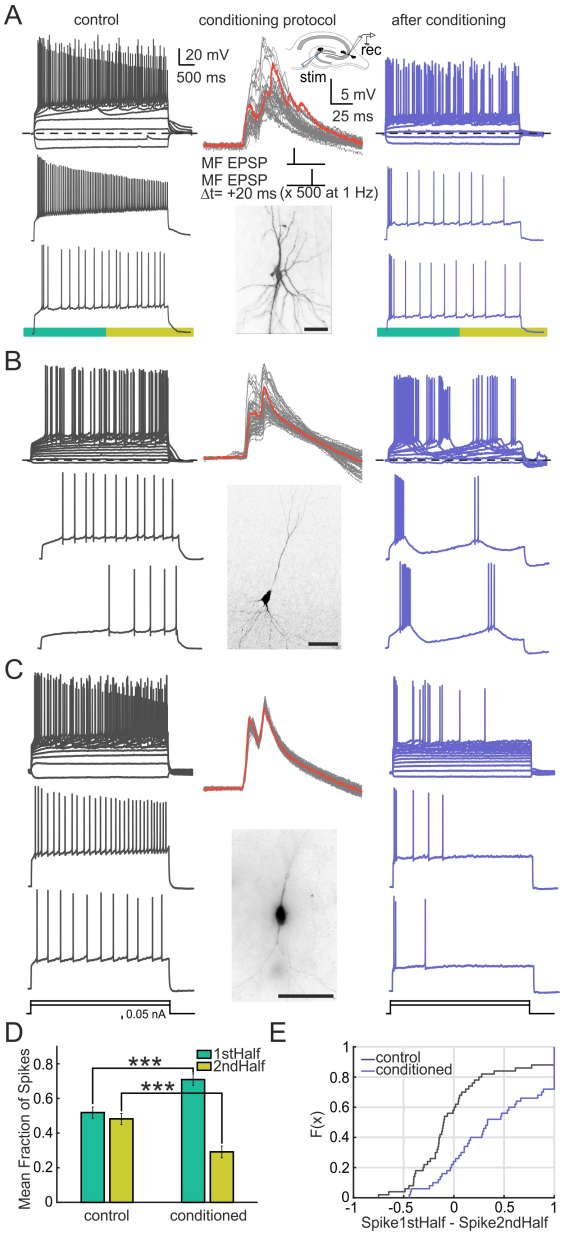

Fig 1. Firing pattern transitions occur in CA3 neurons after subthreshold paired-pulse stimulation of afferents. Three examples of neurons in the CA3 area presenting different morphologies and different firing patterns in control conditions. The discharge patterns were measured by injection of step currents of increasing amplitude. Control measurements (gray traces, left) were followed by stimulation of the mossy fibers. The upper trace shows all voltage traces elicited upon different levels of current injection on that cell. Two sample traces of this set are shown below. EPSPs (middle panel) were evoked in response to a stimulation with double current pulses, separated by 20 ms and repeated 500 times at 1 Hz. The series of repeated pulses are shown superimposed. A sample trace is highlighted in red. The inset shows the configuration of recording and stimulating electrodes (on the CA3 region of the hippocampus and on the dentate gyrus, respectively). Below, the morphology obtained by labeling the cells with biocytin is shown. After the conditioning, patterns were measured again (blue traces, right). A) Pyramidal cell switches from non-adapting burst to intrinsic burst firing. B) Pyramidal cell switches from delay accelerating to intrinsic burst continuous pattern. C) Bipolar cell switches from non-adapting continuous to adapting continuous firing (scale bars = 50μm). D) Mean Fraction of Spikes for the population in the first and second half of the voltage trace (green and yellow rectangle below the trace, respectively) for both control and conditioned cases. A significant redistribution on the fraction of spikes is observed after the conditioning, where the fraction of spikes on the first half is increased while it decreases in the second half (n=50, p=1.92e-6, two-sided Wilcoxon signed rank test). E) Empirical Cumulative Distribution Function for the data shown in D. Every individual cell, for both control and conditioned cases, is represented as the number of spikes for the first half of the trace minus the spikes for the second half (n=50)

bioRxiv preprint doi: https://doi.org/10.1101/084152; this version posted May 11, 2017. The copyright holder for this preprint (which was not certified by peer review) is the author/funder, who has granted bioRxiv a license to display the preprint in perpetuity. It is made available under aCC-BY-NC-ND 4.0 International license.

Results

0.1 Firing patterns of CA3 neurons change after subthreshold stimulation

Whole-cell patch clamp recordings of CA3 neurons were performed in rat hippocampal organotypic cultures. The intrinsic firing patterns of the neurons were recorded before and after conditioning by extracellular stimulation of the mossy fibers originating in the dentate gyrus. The conditioning stimuli consisted of paired pulses (0.1 ms duration pulses, interval 10 – 20 ms) applied at 1 Hz, and repeated 500 times for a total period of approximately 8 minutes. The amplitude of the pulses was adjusted for each recorded cell to elicit only subthreshold excitatory post-synaptic potentials (EPSPs). This mossy fiber stimulation protocol is a modification of that described by Brandalise and Gerber [27, 28], which has been previously shown to elicit heterosynaptic subthreshold plasticity in CA3 pyramidal-pyramidal synapses. The firing patterns of neurons were assessed with a sequence of constant current injections. For convenience, we used the terminology of the Petilla classification [15] to label these patterns. Interestingly, we observed that after the conditioning protocol, the Petilla discharge label had to be adapted for most of the cells, independently of their initial firing type. For example, the pyramidal cell shown in Fig 1A had a non-adapting burst pattern before stimulation (gray traces). After conditioning (blue traces), this response changed to intrinsic burst. The same transition was observed for the pyramidal cell on panel 1B, whose initial pattern was delayed accelerating. The bipolar cell on panel 1C switched from non-adapting continuous to adapting continuous firing. We observed that the most common transition performed by the cells was towards adapting and intrinsic burst patterns. Indeed, the quantification of the mean fraction of spikes in the first half versus the second half of the voltage for the population of recorded cells showed a distribution of the spikes in favor of the first half (Figs 1D, 1E) (n=50). This result supports our observations that the main pattern transitions are towards adapting and intrinsic burst behaviors after the conditioning. These changes in firing pattern were present in most cells immediately after the stimulation protocol, and were stable at least 15 minutes after the stimulation. The mossy fiber conditioning was followed by a significant 36 MΩ (25%) decrease in input resistance (Rin), (from 144.8 ± 73.0MΩ to 108.4 ± 65.3MΩ, two-sided Wilcoxon signed rank test, p=1.1e-5). There was also a significant 5 mV (7%) depolarization of the resting membrane potential (Vm) (-65.3 ± 5.0mV) with respect to resting level (-70.4 ± 5.7mV, two-sided Wilcoxon signed rank test, p=2.3e-5, n = 50). However, the firing pattern changes could not be induced neither by simply holding the resting membrane potential at different values (see Fig S1, n = 10), nor by the step-currents used to measure the discharge patterns (see Fig S1, n = 15). No significant changes in Vm and Rin in cells were found in unconditioned cells (Vm: -69.3 ± 2.0mV, -69.1 ± 1.9mV, paired t-test, p=0.64, Rin: 148.8 ± 56.1MΩ, 158.9 ± 55.6MΩ, paired t-test, p=0.063, n = 15). Intracellular dialysis could also be excluded as the cause of the pattern transitions, as firings did not change spontaneously over time (see Fig S1). In addition, we assessed that the effect was also present under conditions where dialysis was minimized (see Fig S2, n = 15).

0.2 Firing pattern transitions occur also via somatic conditioning and are blocked by protein kinase A and C inhibitors

We attempted to resolve if synaptic input was necessary to elicit the changes, or whether they could be induced directly at the soma. To this end, we used intra-somatic injection of paired step current pulses whose parameters were chosen to elicit a similar

bioRxiv preprint doi: https://doi.org/10.1101/084152; this version posted May 11, 2017. The copyright holder for this preprint (which was not certified by peer review) is the author/funder, who has granted bioRxiv a license to display the preprint in perpetuity. It is made available under aCC-BY-NC-ND 4.0 International license.

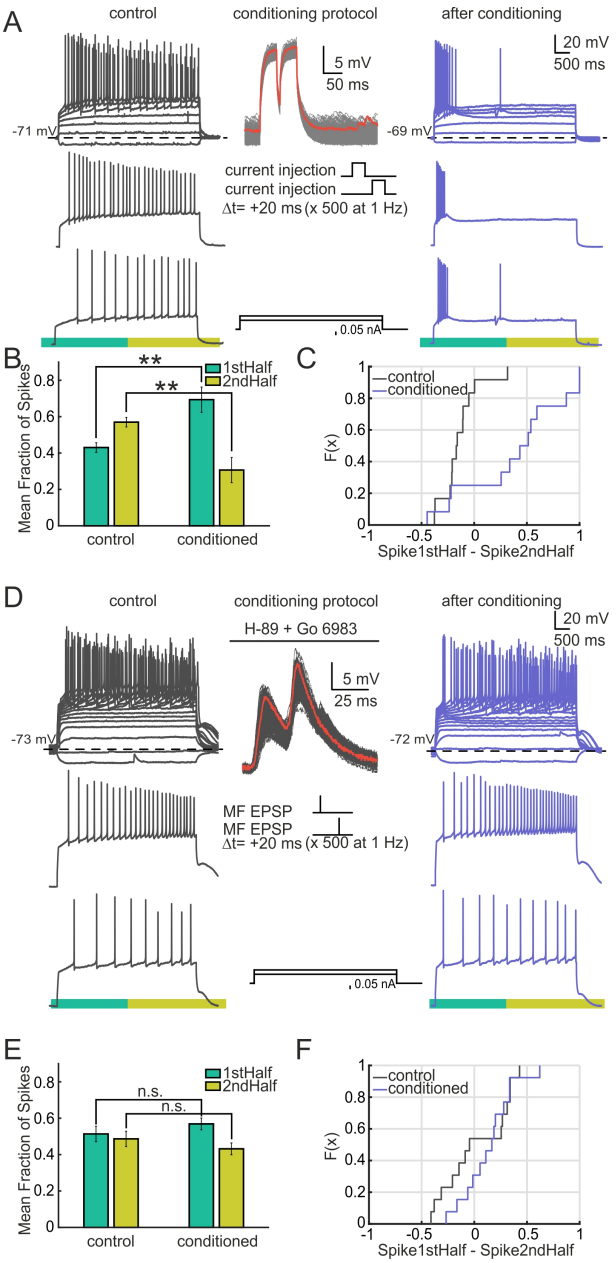

Fig 2. CA3 firing pattern transitions occur upon somatic conditioning and are blocked by kinase inhibitors. A) Example of an intrasomatic conditioned cell that switch from delay accelerating (gray traces) to intrinsic burst firing (blue traces). The conditioning protocol is shown in the middle column. EPSPs were evoked by injection of paired current steps, of 50 ms in duration and separated by 20 ms. The double steps were repeated 500 times at 1 Hz. The series of repeated pulses are shown superimposed. A sample trace is shown in red. B) Mean Fraction of Spikes for the population in the first and second half of the voltage trace for both control and conditioned cases. A significant redistribution on the fraction of spikes occurs after the conditioning. The fraction of spikes on the first half is increased while it decreases in the second half (n=12, p=0.0024, two-sided Wilcoxon signed rank test). C) Empirical Cumulative Distribution Function for the data shown in B. Every individual cell is represented as the number of spikes for the first half of the trace minus the spikes for the second half (n=12). D) Example of a mossy fiber conditioned cell (as described in Fig 1) under the presence of H-89 and Go 6983 (PKA and PKC inhibitors) on the intracellular pipette. The cell presents a delay accelerating pattern in control conditions and remains under such pattern after the conditioning protocol is applied. E) Mean Fraction of Spikes for the population in the first and second half of the voltage trace for both control and conditioned cases. The redistribution of the fraction of spikes was not significant after the conditioning (n=13, p=0.266, two-sided Wilcoxon signed rank test). F) Empirical Cumulative Distribution Function for the data shown in D. Every individual cell is represented as the number of spikes for the first half of the trace minus the spikes for the second half (n=13).

bioRxiv preprint doi: https://doi.org/10.1101/084152; this version posted May 11, 2017. The copyright holder for this preprint (which was not certified by peer review) is the author/funder, who has granted bioRxiv a license to display the preprint in perpetuity. It is made available under aCC-BY-NC-ND 4.0 International license.

somatic voltage response compared to that generated by the mossy fiber stimulation (Fig 2). This direct subthreshold somatic stimulus evoked changes in discharge pattern that were similar to those elicited by the indirect mossy stimulation. The cell in Fig 2A displayed a delay accelerating firing pattern in control conditions and underwent a transition towards intrinsic burst pattern after somatic conditioning. The population data showed a significant redistribution in the fraction of spikes in favor of the first half of the trace versus the second half after the conditioning (Figs 1B and C) (n=12). In this result we observed the same tendency of neurons to become adapting and intrinsic burst after conditioning. Furthermore, due to the nature of the conditioning at the soma, this result also suggests that the mechanism inducing the firing pattern change is not localized to synapses, but rather acts at a more central, probably somatic or proximal dendritic level. We next sought to identify what internal mechanism could be responsible for the firing pattern transitions. The firing pattern of the cell depends on the distribution of membrane ion channels that the cell presents at its membrane [18]. A possible mechanism would act upon this distribution. Due to the time scale of the response (on the order of minutes) we ruled out protein synthesis of new channels on the membrane. An alternative would be channel phosphorylation, a mechanism known to affect the conductance on a relatively short timescale [29]. We reproduced the conditioning protocol in the presence of the PKA and PKC inhibitors H-89 and Go 6983 in the intracellular recording pipette. On Fig 2D a cell whose firing pattern in control conditions was delay accelerating is shown. After mossy fiber conditioning in the presence of the inhibitors the cell remained under this pattern. 84% of cells showed no visible modulation of the Petilla label pattern (11 out of the 13 cells). Panels 2E and F show the population response for cells stimulated under these conditions. No significant redistribution of the spikes was found on the presence of the inhibitors (n=13). These results suggest that phosphorylation is implicated in the mechanism of firing pattern transition.

0.3 Cluster analysis of experimental traces: quantification of identity changes in neurons

We observed that the conditioning induced firing pattern changes from more regular patterns towards early bursting and adapting patterns. We sought to quantify these changes using hierarchical clustering methods [16, 30, 31] to establish more objectively which discharge type to associate to every response, and to quantify the frequencies of transitions between them. Previous studies have used clustering methods to quantify the similarity between vectors of features extracted from the voltage traces, such as action potential (AP) amplitude, firing rate, or accommodation index [16, 30, 31]. However, those metrics are not suitable for of our dataset, because several features commonly used in those methods are unaffected by the conditioning. For example, AP amplitude, width and afterhyperpolarization (AHP) showed no difference before and after the stimulation (AP amplitude: 78.63 $\pm$ 14.95mV, 75.60 $\pm$ 9.77mV, paired t-test, p=0.11, AP half width: 1.11 $\pm$ 0.26ms, 1.10 $\pm$ 0.24ms, paired t-test, p=0.74, AHP: 13.62 $\pm$ 3.76mV, 12.66 $\pm$ 4.15mV, paired t-test, p=0.12, n = 50). Consequently, we chose to use Dynamic Time Warping (DTW) as a comparison measure, because it operates directly on the action potential sequence rather than relying on a pre-defined set of features (see Methods for a detailed explanation). Feature vectors of the instantaneous firing rate of the voltage traces were compared pairwise using the DTW algorithm. As an internal control, vectors coming from the same set of step current injections of a cell were treated independently. The results of the cluster analysis of discharge patterns are shown in Fig 3. We set the threshold of the clustering tree at a level that separates the traces into 5 distinct families. The threshold was chosen large enough to yield sufficient structure to

bioRxiv preprint doi: https://doi.org/10.1101/084152; this version posted May 11, 2017. The copyright holder for this preprint (which was not certified by peer review) is the author/funder, who has granted bioRxiv a license to display the preprint in perpetuity. It is made available under aCC-BY-NC-ND 4.0 International license.

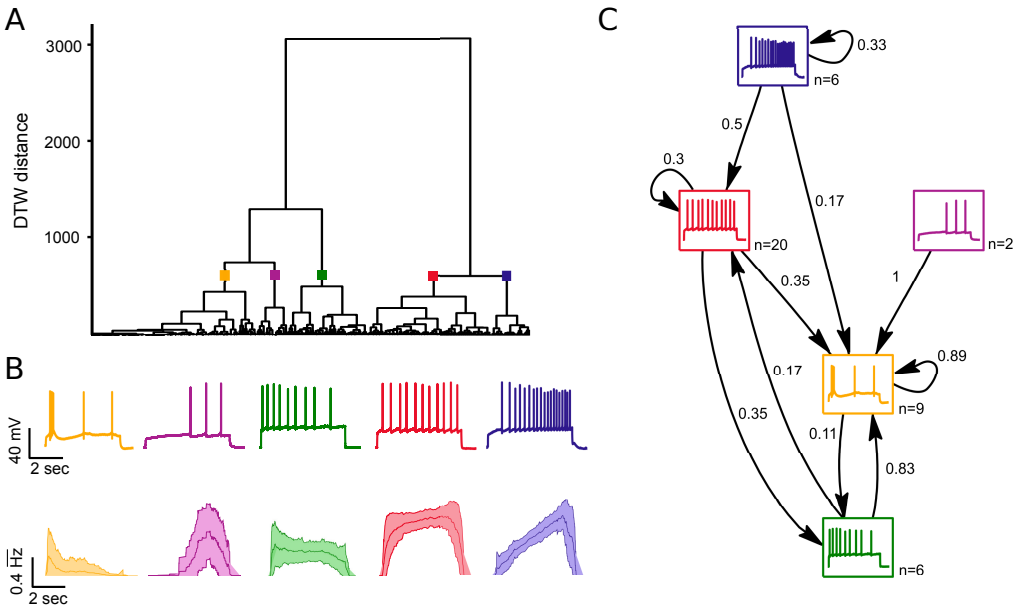

Fig 3. Hierarchical clustering of experimental discharge traces. A) Dendrogram of clustered traces. The data included in the cluster corresponds to the mossy fiber conditioned cells of Fig 1. Two main families can be identified: one containing adapting and bursting traces, together with delayed spiking patterns (left branch); and another branch containing regular and accelerating traces (right branch) (n=50). B) Representative traces from each cluster. Below, average instantaneous firing rate over all traces belonging to the same cluster. Middle lines indicate the mean; light outer lines indicate standard deviations. The instantaneous firing rate (in Hz) is normalized to 1. C) Transitions observed between firing patterns before and after conditioning. Each cell is assigned to a single cluster (represented as a box) for both the control and conditioned cases. Arrows indicate transitions between types whenever a cell changed cluster. Self-loops indicate that the firing pattern was retained after conditioning. Numbers indicate percentages of observed transitions, and the number of cells in each category under control conditions is displayed next to each pattern type. Cells tend to transition towards adapting and bursting patterns following conditioning (n = 43). Seven cells were assigned as unclassified.

bioRxiv preprint doi: https://doi.org/10.1101/084152; this version posted May 11, 2017. The copyright holder for this preprint (which was not certified by peer review) is the author/funder, who has granted bioRxiv a license to display the preprint in perpetuity. It is made available under aCC-BY-NC-ND 4.0 International license.

interpret the hierarchy in terms of recognized response types [15]. Representative traces of each family are shown in Fig 3B. The average of the firing rate vectors of every cluster is depicted beneath each representative trace. The clustering algorithm captures well the typical time courses of the firing patterns. The right branch of the cluster tree contains accelerating and non-adapting firing patterns, while the other contains adapting and intrinsic bursting patterns together with a smaller group of traces that have delayed spiking profiles (Fig 3A). The consistency of the algorithm was confirmed by its successful clustering of independent feature vectors derived from the same set of current injections (same cell under the same conditions) into a single cluster. Indeed, in 86% of cases (43 of the 50 cells) the algorithm successfully allocated the majority of vectors from the same set of current injections into single clusters. Vectors from the 7 remaining cells were not consistently classified. For 50% of the cells all of their voltage traces fell into the same cluster, and for 90% of the cells at least 50% did (see Fig S3). The allocation of some responses from the same cell into more than a single cluster does however follow a biological logic. For example, for cells classified as accelerating, some of their voltage traces could reasonably fall into the non-adapting cluster because acceleration may vanish at high current injections. A similar reasonable misclassification is possible for adapting traces. In this case low current injections may be classified as non-adapting because the currents are not high enough to elicit adaptation (see Fig S4). In particular, many of the traces belonging to the delayed spiking cluster come from cells whose traces at low current injections were assigned to the accelerating cluster, or belonged to non-adapting cells with spiking delay. The transitions between cluster types induced by the stimulation protocol are shown in Fig 3C. This figure considers only those cells in which responses both before and after conditioning could be clearly assigned to a cluster. In total, 68% of the cells (n = 50) changed their original cluster as a result of subthreshold conditioning. This quantitative result supports the qualitative observation that cells tend to transition towards more adapting and intrinsic burst profiles. 70% of cells initially belonging to the non-adapting cluster exhibited such changes in response (14 cells), with 35% moving into the intrinsic burst category, and 35% exhibiting adapting spike patterns. 5 of the 6 cells from the adapting cluster (83%) switched to the intrinsic burst type. Most of the cells for which the firing pattern did not change were already in the most common target states of transitions. For example, 89% of the intrinsic bursting cells did not change cluster. This provides further evidence for a predominantly unidirectional change of firing patterns in response to conditioning. The 7 cells that could not be consistently classified under control conditions were all correctly classified after the stimulation. They showed the same transition tendencies: 5 moved into the intrinsic bursting cluster, the other 2 became adapting.

0.4 A conductance based model explains the transitions between firing patterns

The consistent transition towards adapting and intrinsic bursting behaviors suggests a common underlying mechanism for most cell types. Our results showing that phosphorylation inhibition blocks firing pattern change after conditioning (Fig 2) support the hypothesis that the prime candidate for this mechanism is a change in the profile of active conductances contributing to action potential discharge dynamics. We explored this possibility using simulations of action potential discharge in a conductance-based single compartment neuron model containing 9 voltage and calcium gated ion channels (see Methods). The densities and kinetics of these channels were derived from experimental measurements of CA3 pyramidal neurons [12]. We tuned only their maximum conductances to reproduce the discharge patterns observed in our experiments. The allowed ranges of maximum conductances were restricted to those

bioRxiv preprint doi: https://doi.org/10.1101/084152; this version posted May 11, 2017. The copyright holder for this preprint (which was not certified by peer review) is the author/funder, who has granted bioRxiv a license to display the preprint in perpetuity. It is made available under aCC-BY-NC-ND 4.0 International license.

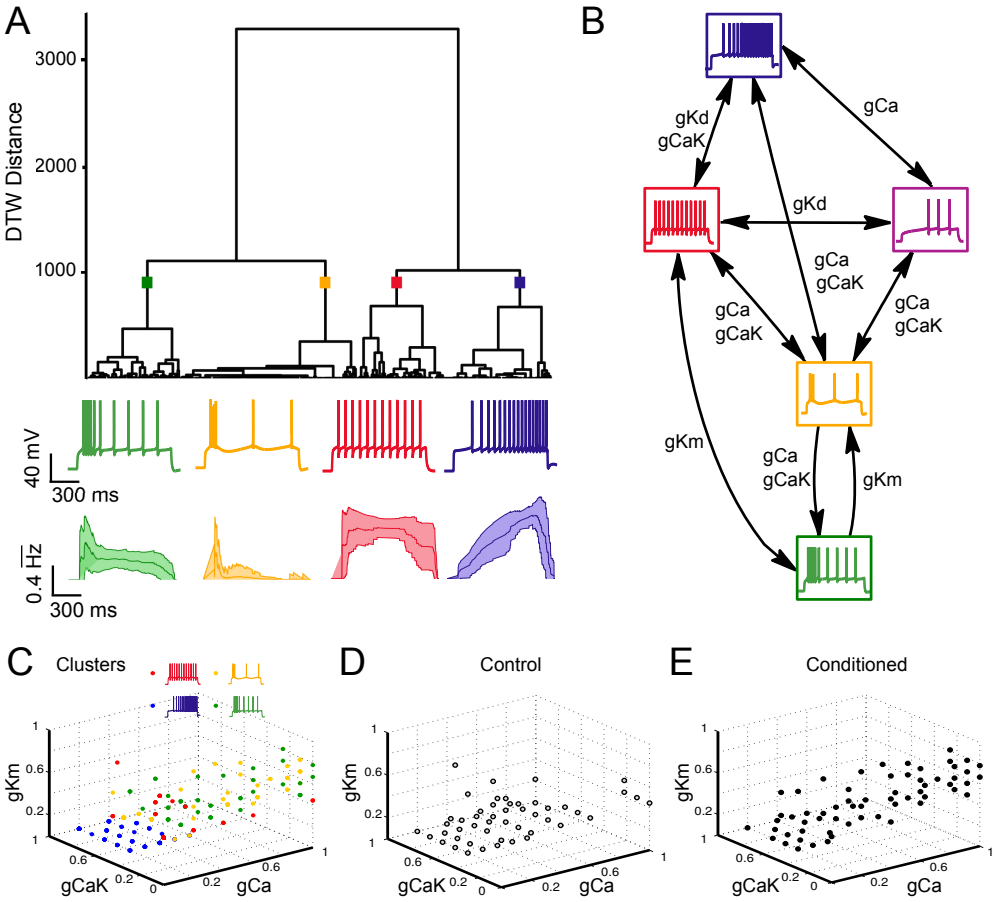

Fig 4. Hierarchical clustering of the model-generated discharge traces mapped to the experimental traces. Every experimental trace was matched to a model trace using the DTW algorithm as a search tool on a model database of traces. Hierarchical clustering was then applied to the model traces. A) The clustering algorithm distinguishes four main families, which correspond to adapting, intrinsic burst, non-adapting and accelerating patterns. Below the dendrogram, a representative model trace of every cluster is depicted. The single compartment model could reproduce the sample experimental traces of Fig 3. The exact conductance values used to produce every model pattern and the amount of current injection are shown in the Table S1. Underneath, average instantaneous firing rate within each cluster with its standard deviation (n = 50) B) Conductance road map showing the key conductances responsible for a transition in firing pattern on the model generated traces. The main channels implicated are gCa, $gCaK$, gKd and gKm. C) Distribution of the conductance vectors of the model traces clustered in (A) in 3D space. Axes correspond to: calcium conductance variable (gCa); calcium-dependent potassium channel ($gCaK$); and potassium channel (gKm). The dots are color coded according to their cluster assignment. D) Distribution of the conductance vectors in 3D space of the model traces matched to cells in control conditions E) Distribution of the conductance vectors of traces matched to cells after conditioning. Conditioned cells present a higher content of gCa and gKm.

bioRxiv preprint doi: https://doi.org/10.1101/084152; this version posted May 11, 2017. The copyright holder for this preprint (which was not certified by peer review) is the author/funder, who has granted bioRxiv a license to display the preprint in perpetuity. It is made available under aCC-BY-NC-ND 4.0 International license.

reported in the literature [12]. In order to explain the experimental transitions, we compared the performance of the clustering procedure on the model and the experimental data. In a first step, the maximal conductance densities of the model were tuned to match the various experimentally observed firing patterns. This tuning was performed manually, and the match to the traces was qualitative. The absolute values for the conductances required to match the main experimental categories (Fig 3: adapting, intrinsic burst, delay spiking, accelerating and non-adapting) are reported in Table S1. We also were able to reproduce the experimental traces in the morphologically realistic model described by Hemond et al. [12] (see Fig S5). Although the maximal conductance values had to be adjusted to satisfy the different impedance of the more detailed morphology, the same key channels are responsible for each category of firings both the single compartment and in the realistic CA3 model. In a second step, a database of representative ranges of conductances that could plausibly explain the discharge patterns observed experimentally was generated using the single compartment model. To do this, the maximal conductances of the different channels were swept through ranges that would likely encompass the experimentally observed patterns (see Table S2 for the exact ranges). In this way a total of 861 conductance profiles were generated. We obtained the discharge response to different levels of current injection for each conductance profile, giving a total of 5166 voltage traces with their associated conductance profiles. Every single experimental trace (coming from both, control and conditioned cases) was matched against the collection of traces in the model database using the DTW algorithm. The best fit was then selected, allowing us to obtain an estimate of the conductance profile likely to be present in the experimental neuron. These estimates also define the subset of model traces that best represent their experimental counterparts. This subset was then fed to the same hierarchical clustering procedure that was previously performed for the experimental data (Fig 3). The result of hierarchical clustering of the model traces is shown in Fig 4A. There are four main families, corresponding to adapting, intrinsic bursting, accelerating and non-accommodating behavior. The classification of the model traces is very similar to the experimental one. We noted however the absence of the small class of delayed-spiking patterns (second cluster of Fig 3), which in the case of the model were allocated mostly to the accelerating cluster. The transition diagram of Fig 4B represent the crucial conductances determining the transitions between discharge patterns, obtained during the first step of manual tuning. These are gKm, $gCaK$, gCa and gKd. In this manner, for the delayed discharge pattern, the presence of gKd is required for a delayed onset of the spiking, and the slow inactivation of gKd is important for generating the accelerating discharge pattern. In the case of the adapting and intrinsic burst patterns, the inclusion of gKm and gCa (given the presence of basal levels of $gCaK$) is necessary for the slowing down of the action potentials after the initial discharge. In panel 4C each point indicates the location of an experimental discharge response matched to the model in conductance space. The color of a point shows its cluster assignment. There is a systematic segregation of the data, indicating how the discharge classes of Fig 4A conform to localized regions of conductance space. This correspondence of firing patterns and biophysical parameters offers an interpretation of the causes of transitions between firing behaviors induced by mossy fiber stimulation (Fig 3C). The shift towards adapting and intrinsic bursting behavior after the conditioning corresponds to an increase in calcium related, and gKm conductances (Figs 4D,E).

bioRxiv preprint doi: https://doi.org/10.1101/084152; this version posted May 11, 2017. The copyright holder for this preprint (which was not certified by peer review) is the author/funder, who has granted bioRxiv a license to display the preprint in perpetuity. It is made available under aCC-BY-NC-ND 4.0 International license.

1 Discussion

We have shown that the characteristic firing patterns of neurons in the CA3 region of the hippocampus can be modified by subthreshold stimulation of the soma. The effect was elicited either indirectly by stimulation of the mossy fibers, or directly by somatic current injection. The change was present immediately after the 8 minute conditioning protocol, suggesting that the mechanism underlying the transition operates on a timescale of at most, a few minutes. The effect was abolished under the presence of PKA and PKC inhibitors, indicating that phosphorylation of conductance channels over the duration of the conditioning is necessary for the firing pattern changes. Hierarchical cluster analysis showed that the transitions observed are more likely towards adapting and intrinsic burst responses. We were able to reproduce the experimentally observed changes in firing in simulations of a conductance-based model of neuron electrophysiology. We found that the shift in responses towards adapting and intrinsic burst can be explained by recruitment of calcium and M-type potassium conductances. These results indicate that suprathreshold discharge behavior of neurons on the time scale of seconds can be modified by the statistics of ongoing subthreshold activity on a much longer time scale.

1.1 Previously reported changes in firing pattern

Activity dependent changes on the intrinsic firing properties of neurons have been reported extensively, although the attention has been restricted primarily to the modulation of firing rates for homeostatic plasticity [20, 32–34]. Regarding the dynamics of the discharge, plasticity has been reported in lobster, with activity isolation being a crucial component in shaping the patterns [35]. Modulation of the delay spiking pattern in the hippocampus [36, 37] and in the cortex [26] have been shown to be induced by network activity or conditioning pulses. Induction of the burst pattern after status epilepticus has also been reported in hippocampus [38] while Thompson and colleagues [39] have shown reductions in post-burst AHP and accommodation in CA3 neurons after eye-blink conditioning. These studies favor the hypothesis that is the current network status of CA3 the responsible of shaping the discharge pattern of neurons in this region. In this manner, the firing pattern transitions that we observe are likely to be elicited when disturbing the basal activity that the neurons were receiving on the CA3 network.

This study was performed on organotypic cultures, derived from brain slices of newborn rats that are incubated for three weeks using the roller-tube technique [40]. Organotypic cultures have been used extensively to characterize electrophysiological properties of hippocampal neurons and it is know that the tissue preserves the anatomical organization of the adult hippocampus, as well as its connectivity and characteristic spontaneous activity [41, 42]. Most of the studies cited in this chapter were done in cultures or juvenile acute brain slices, indicating that the plasticity of the patterns is not unique to the organotypic preparation. It would be interesting to know however whether this type of plasticity is also prominent in the adult brain and if it also happens, at the same time scale, in other brain areas such as the cerebral cortex.

1.2 Modulation of cell excitability via conductance changes

Activity dependent changes of conductance have been extensively studied, and shown to be triggered even by learning paradigms [39, 43, 44]. The work of Turrigiano et al. [35] suggested that a calcium dependent mechanism could modulate the neural conductances in STG lobster neurons, and that this would translate into changes in the cells' firing patterns. Later work showed that depolarizing pulses at 1Hz could alter the density of

bioRxiv preprint doi: https://doi.org/10.1101/084152; this version posted May 11, 2017. The copyright holder for this preprint (which was not certified by peer review) is the author/funder, who has granted bioRxiv a license to display the preprint in perpetuity. It is made available under aCC-BY-NC-ND 4.0 International license.

the calcium-dependent outward current $ICaK$ and the transient outward current IA in the STG [45]. These studies led to theories of homeostatic plasticity [20,33], which propose that cells maintain both the turnover of ion channels, and a stable level of activity, to compensate for changes in synaptic strength. However the time scale of such mechanisms typically extends over hours, and presumably involves processes of gene expression [46], whereas in our experiments the changes were observed immediately after conditioning. Aizenman and Linden [47] observed rapid changes of excitability of cerebellar cells after synaptic stimulation, and proposed a calcium-dependent modification though phosphorylation of $gCaT$ and $gCaK$ to account for the observed changes. Interestingly, these are the same candidate channels that we have identified as underlying the discharge pattern changes in this study. Supporting these lines, rapid up- or down-regulation of ion channel conductance via phosphorylation or vesicle modulation due to calcium signaling has been extendedly demonstrated [22,29,43] and it has been shown that ion channels possess a complex of scaffold proteins containing certain protein kinases that could selectively regulate channel conductance through phosphorylation [29]. This mechanism could provide a link between the activity of the network and the specific conductance recruitment. An alternative explanation to the conductance recruitment is that continuous stimulation of the neuron may alter the ion concentrations in the cellular environment; for example, by altering intracellular potassium and calcium concentrations [48,49]. However, our simulations show that the decay time constant of the intracellular calcium is too short to allow significant accumulation over the period of conditioning (see Fig S6A-C). Even if the time constant were greatly increased, the accumulation of calcium during conditioning would be insufficient to elicit a significant change in firing pattern (see Fig S6D). Regarding potassium, our extracellular concentration was less than that required [48] for the changes in pattern that we observe. On the other hand, the abolition of the effect by the inhibition of phosphorylation points towards an induction of a biochemical pathway as the cause of the conductance increase.

1.3 Candidate conductances for the firing pattern transitions

Our model suggests that the likely candidates for eliciting any type of transitions through the firing pattern space of CA3 cells are gKd, gKm and gCa coupled with $gCaK$. We are aware that alternative channels could elicit a similar dynamical response. The effect on the spike delay mediated by a slow inactivating hyperpolarizing current, such as gKd can also be elicited by a slow non-inactivating depolarizing current such as $gNap$. Thus, it is possible that different cells recruit different set of conductances depending on their initial conductance profile. However, the candidates we propose have been previously reported to shape the spiking response of the cell via activity dependent mechanisms. For example, it is well established in the epilepsy literature that $gCaT$ is strongly associated with the switch to bursting mode in hippocampal cells [38,50] while gKd in the hippocampus and similar potassium conductances in the cortex have been shown to be up- or down-regulated according to network activity and modulate the delay firing response of the cell [26,36,37]. Modulation of the M-type current upon activity has also been shown in the hippocampal region CA1 [51] and in CA3 [52], with the latter group reporting that transient subthreshold depolarizing pulses are more effective in the modulation of the current.

The conditioning protocol elicited stereotypic transitions of pattern towards adapting or intrinsic burst patterns. However, it was not equally likely for all cell types to perform such transitions. For example, accelerating cells moved towards regular patterns with higher probability than the rest of patterns (Fig 3C). We speculate that either the initial density of channels favors the different likelihood of transitions, or that a cell on such initial state must necessarily become regular during the transition to any

bioRxiv preprint doi: https://doi.org/10.1101/084152; this version posted May 11, 2017. The copyright holder for this preprint (which was not certified by peer review) is the author/funder, who has granted bioRxiv a license to display the preprint in perpetuity. It is made available under aCC-BY-NC-ND 4.0 International license.

other pattern. An alternative is that there may be some cell types that obey distinct rules. For example, we noticed that 4 cells from the non-adapting cluster had high firing rates under control conditions (see Fig S7). Two of these had smooth cell morphologies. The other two cells correspond to very densely spiny cells, with stellate morphologies. Interestingly, although transitions towards bursting or classic adapting behaviors were not observed on these cells, there was a modulation on the delay of the first spike in both cell types, suggesting that the stimulation protocol had a differential effect on this particular neural population.

One of the typical transitions that we observe in our dataset is the switch of cells towards bursting behaviors. We emphasize that this is not the only transition that is induced, but special attention should be given to the burst mechanism. It is known from the literature that different types of cells can present this dual behavior. For example, relay cells on the thalamus become bursty upon hyperpolarization because of T-type conductance inactivation [53]. In our case, after the induction protocol, the cells depolarized 5 mV in average, so we rule out this hyperpolarization mechanism. The main form of discharge of CA3 cells have been known to be either regular or bursting [12]. Although the firing pattern transitions were abolished in the presence of PKA and PKC inhibitors, 2 cells out of 13 showed still transitions to intrinsic burst. This could be likely due to failure of diffusion of inhibitors from the electrode, but we cannot exclude a different mechanism for this type of transition (for example, through different kinase pathways).

1.4 Functional implications of firing pattern modulation

The fact that neurons possess the internal machinery to mediate the observed transitions raises questions about the computational consequences of such behavior. As proposed by Shin et al. [54], a neuron that can dynamically adapt its output firing in response to its input statistics would have important advantages. If such neuron could adjust its threshold and dynamic range upon activity, it could respond to stimuli over a broad range of amplitudes and frequencies without compromising the sensitivity and dynamic range of the cell. Spike frequency accommodation has the characteristics of a high-pass filter [55]. Since our conditioning stimuli occurred at constant frequencies, the cells may have recruited a specific set of conductances that shift their integration properties so as to gain sensitivity in the new spectrum range. Differences in filtering properties of brain stem neurons have also been shown to facilitate the extraction of spatial information from natural sounds [56] and most of the conductances that we identify in this study have been shown to be frequency resonance candidates [57–59]. These resonance properties of cells may have important functional implications for neural activity and brain rhythms [60, 61]. In addition, modeling studies have shown that a neuron able to adapt to its own input statistics is able to maximize the mutual information between its input and output firing rates [62]. This type of effect can emerge following firing rate homeostasis rules and promote metaplasticity [63]; on the other hand it can be their cause [64]. Finally, this fast adaptability of the firings may also be important for specific memory acquisition on the hippocampus [39, 65]. Further studies will be needed in order to unravel the role that such firing pattern transitions may have for computations in neural circuits. A first step towards this goal must be to explore more generally how the form and frequency spectrum of somatic input signals on the long time scale affect the distinct firing patterns that neurons exhibit on the short scale.

bioRxiv preprint doi: https://doi.org/10.1101/084152; this version posted May 11, 2017. The copyright holder for this preprint (which was not certified by peer review) is the author/funder, who has granted bioRxiv a license to display the preprint in perpetuity. It is made available under aCC-BY-NC-ND 4.0 International license.

2 Conclusion

We have shown that hippocampal neurons in rat organotypic cultures can rapidly adapt their supratheshold action potential discharge patterns in response to subthreshold paired pulse conditioning stimuli delivered to their somata either by activation of their synapses, or directly by intrasomatic current injection. We propose that these changes are mediated via phosphorylation by recruitment of calcium and M-type potassium conductances, conditional on the statistics of their somatic input currents. Such a mechanism would allow the neuron to adapt its output behavior to the requirements of the network in which it is embedded. Our results also imply that the discharge characteristics of neurons in this hippocampal region are not constant and may not provide a reliable descriptor of a neural phenotype.

Materials and Methods

All experiments were conducted in accordance with guidelines and regulations of the cantonal veterinary office of Zurich; License Nr 81-2014.

2.1 Electrophysiological Recordings

Rat hippocampal organotypic cultures [40] of average postnatal age 21 days were transferred to a recording chamber and mounted on an upright microscope (Axioskop FS1; Zeiss). The cultures were superfused with an external solution ($pH7.4$) containing (in mM) 148.8 Na^+, 2.7 K^+, 149.2 Cl^-, 2.8 Ca^{2+}, 2.0 Mg^{2+}, 11.6 HCO_3^-, 0.4 $H_2PO_4^-$, 5.6 D-glucose, and 10 mg/l Phenol Red. All experiments were performed at 34 °C. Whole-cell recordings of CA3 neurons were obtained with patch pipettes (4-7 $M\Omega$). Pipettes were filled (in mM) with 126 Kgluconate, 4 $NaCl$, 1 $MgSO_4$, 0.1 $BAPTA-free$, 0.05 $BAPTA-Ca^{2+}$, 15 glucose, 3 ATP, 5 $HEPES$ (pH was adjusted to 7.2 with KOH) 0.1 GTP, and 10.4 byocitin. IPSPs in the recorded cells were reduced by adding picrotoxin (1 mM) to the intracellular patch solution in order to elicit reliable depolarization in the cell.

The recording pipettes were manually positioned under microscope control. Recorded neurons were located mostly in the pyramidal cell layer. Electrophysiology and subsequent histology in a subset of the cells recorded suggest that the neurons described below include both pyramidal cells and smooth cells.

Current-voltage relationships were determined by step command potentials and had duration of 1 s to ensure steady-state responses. Data were recorded using an Axopatch 200B amplifier (Molecular Devices). Series resistance was monitored regularly, and was typically between 5 and 15 $M\Omega$. Cells were excluded from further analysis if this value changed by more than 20% during the recording. Junction potential and bridge was not corrected.

Mossy fibers were stimulated with a bipolar tungsten electrode. The intensity of the stimulus was adjusted to evoke subthreshold post-synaptic potential responses of 15 mV on average in the recorded neuron (minimal stimulation + 20% stimulation intensity).

Action potential discharges were evoked by injected current steps (-0.08 up to 1.8 nA; step increment 0.05 - 0.15 nA, depending on the input resistance of the recorded cell) each lasting 5 seconds. After this control, the neurons were conditioned by mossy fibers activation, consisting of a double pulse (0.1 ms duration pulses, interval 10 - 20 ms) at a frequency of 1 Hz, repeated 500 times. Thus, the conditioning period was approximately 8 minutes. Immediately after this conditioning, the firing pattern of the neuron was assessed again using the same step protocol. The step protocols were repeated 3 times with 5 min intervals to assess stability. In a subset of experiments,

bioRxiv preprint doi: https://doi.org/10.1101/084152; this version posted May 11, 2017. The copyright holder for this preprint (which was not certified by peer review) is the author/funder, who has granted bioRxiv a license to display the preprint in perpetuity. It is made available under aCC-BY-NC-ND 4.0 International license.

mossy fiber subthreshold responses were mimicked by injecting somatically and at a frequency of 1 Hz double step current pulses of 50ms of duration and 20ms of interstep interval. The amplitude of the pulse was adjusted in order to get a depolarization of 15 mV on average.

2.2 Histology

Hippocampal slice cultures were prepared for morphological assessment by fixing in freshly prepared 4% paraformaldehyde in 0.1 M phosphate buffer (PB) at pH 7.4 overnight at 4 °C; washing three times in phosphate-buffered saline (PBS, 1.5 mM KH_2PO_4, 8.5 mM Na_2HPO_4, 137 mM $NaCl$, and 3 mM KCl, pH 7.4); and permeabilizing at room temperature in PBS that contained 10% heat-inactivated donkey serum, and 1% Triton X-100. Then they were incubated overnight at 4 °C with streptavidin conjugated with Alexa (546λ). The cultures were washed again three times in PBS, and then mounted in Fluorostab (Bio-Science Products AG, Emmenbrucke, Switzerland) and coverslipped. High-resolution images were obtained using laser scanning confocal microscopy (Leica TCS SP2, Leica Microsystems, Heidelberg, Germany).

2.3 Data analysis

Signals were digitized at 4 kHz for current clamp and 5 kHz for voltage clamp. These data were analyzed off-line using pCLAMP 10 (Molecular Devices) and MatlabR2011b (MathWorks). Analysis of the voltage traces was performed similar to Chen et al. (2015). The average resting membrane potential of each neuron was estimated as the mean membrane potential during the first 100 ms of current-injection protocol (before injection of the step-current pulses). Input resistance was obtained by measuring the voltage drop across the hyperpolarizing trace of the step-current pulses. APs were located using median filtering, and the threshold was inferred as the point at which the derivative of the voltage trace exceeded 5 mV/ms. AP amplitude was measured from threshold-to-peak and AP afterhyperpolarization (AHP) from the threshold-to through. Half-width was estimated as the full width at half-maximal amplitude. Statistical comparisons between conditions were performed using either a paired t-test or a two-sided Wilcoxon signed rank test, after checking the data for normality using a one-sample Kolmogorov-Smirnov test.

2.4 Cluster analysis of discharge traces

The firing patterns of the neurons were categorized by hierarchical clustering of their discharge patterns. The dataset consisted of all voltage traces recorded from neurons in response to step-wise current injections with different amplitudes, including recordings before and after conditioning. For any one neuron, the collection of responses to different current injections represents the signature of the electrical type. However, for inherent verification of our cluster procedure, we chose to treat each response independently. In this way successful clustering could be confirmed by its ability to assign responses from the same neuron into the same category.

The clustering measured similarity of a feature vector derived from the voltage traces. First the recorded voltage traces were converted into a time series of the instantaneous firing rates. The instantaneous firing rate at each spike was taken as 1/Inter-spike-Interval (ISI). Then the instantaneous rates where linearly interpolated across the spike times at 1 ms time intervals over 6 seconds (5 second current injection step, plus 1 second on and offset), and normalized by the maximum firing rate. Finally, a characteristic feature vector of a common length of 600 elements was obtained by

bioRxiv preprint doi: https://doi.org/10.1101/084152; this version posted May 11, 2017. The copyright holder for this preprint (which was not certified by peer review) is the author/funder, who has granted bioRxiv a license to display the preprint in perpetuity. It is made available under aCC-BY-NC-ND 4.0 International license.

down-sampling the interpolated rate traces by a factor of 10, in order to make them computationally tractable to the similarity measurement.

Similarity distances between pairs of traces were calculated using the Dynamic Time Warping (DTW) measure [66]. DTW takes into account that two similar signals can be out of phase temporarily, and aligns them in a non-linear manner through dynamic programming [67]. The algorithm takes two time series $Q = \langle q_1, q_2, \ldots, q_n \rangle$ and $C = \langle c_1, c_2, \ldots, c_m \rangle$ and computes the best match between the sequences by finding the path of indices that minimizes the total cumulative distance

$$\mathrm{DTW}(Q, C) = \min \sum_{k=1}^{K} w_k \tag{1}$$

where w_k is the cost of alignment associated with the kth element of a warping path W. A warping path starts at q_1 and c_1 respectively, and finds a monotonically increasing sequence of indices i^k and j^k, such that all elements q_i in Q and c_j in C are visited at least once, and for the final step of the path $i^{end} = n$ and $j^{end} = m$ holds. The optimal DTW distance is the cumulative distances $y(i, j)$, corresponding to the costs of the optimal warping path $\langle q_1, \ldots, q_i \rangle$ and $\langle c_1, \ldots, c_j \rangle$. This distance can be computed iteratively by dynamic programming:

$$y(i, j) = d(q_i, c_j) + \min\{y(i-1, j-1), y(i-1, j), y(i, j-1)\} \tag{2}$$

where $d(q_i, c_j)$ is the absolute difference between the elements of the sequence. The optimal warping path is obtained by backtracking from the final element $y(n, m)$, and finding which of the three options (increasing i only, increasing j only, or increasing i and j simultaneously) led to the optimal warping distance, until $i = 1, j = 1$ is reached. A warping window constraint of 10% of the vector size was chosen [67].

The pairwise DTW distances were used to perform hierarchical clustering by Ward's algorithm [68]. The number of classes increases with the level of the hierarchy. We choose to cut the tree at a level that provided sufficient structure to interpret the hierarchy in terms of recognized response types (for example, Ascoli et al. [15]).

Every recording for a given cell was treated as an independent observation, and could in principle be assigned to any cluster. If the electrophysiological state of the cell is expressed in all of its responses, then we expect that all the independent observations derived from that cell should be assigned to the same cluster. However, traces derived from current injections to the same cell in different conditions (pre- or post-stimulation) are expected to be assigned to different clusters if there is significant change in the underlying electrophysiological state.

In fact the independent traces did not cluster perfectly. Instead, the majority of independent observations derived from a given state clustered together and there were a few that fell into other clusters. Therefore, we chose to label the electrical type of each cell according to the cluster that contained the mode of the traces for one set of current injections. Cells for which no clear dominant cluster could be identified, e.g. because half of the traces fell into one cluster, and half of them into another, were labeled as unclassified. A cluster transition was recognized whenever the cell was assigned to different clusters before and after the stimulation protocol.

The analysis was performed using custom-written software in MatlabR2011b. The implementation of the DTW algorithm was obtained from Matlab Central (http://www.mathworks.com/matlabcentral/fileexchange/43156-dynamic-time-warping–dtw).

bioRxiv preprint doi: https://doi.org/10.1101/084152; this version posted May 11, 2017. The copyright holder for this preprint (which was not certified by peer review) is the author/funder, who has granted bioRxiv a license to display the preprint in perpetuity. It is made available under aCC-BY-NC-ND 4.0 International license.

2.5 Neuron simulation model

A single cylindrical compartment, conductance-based neuronal model was used for all simulations. The length and diameter of the cylinder are set at equal dimensions to avoid spatial discretization problems in a single compartment [69, 70]. The passive properties associated with the model were obtained from Hemond et al. [12]. We set the length and diameter of our compartment to 50 μm. The active properties were modeled by including appropriate voltage and calcium gated ion channels whose density and kinetics were obtained from experimental recordings performed in CA3 neurons [12]. The simulations were performed using NEURON [71]. We choose an integration step of 25 μs, which was approximately 1% of the shortest time constant in the model. The voltage- and time-dependent currents followed the Hodgkin and Huxley formalism (1952):

$$C \cdot \frac{\mathrm{d}V}{\mathrm{d}t} = -(I_{Na} + I_{Kdr} + I_{Kd} + I_{KA} + I_{Km} + I_{CaK} + I_{CaL} + I_{CaT} + I_{CaN} + I_{Leak}) \quad (3)$$

Each current I_x is described by the equation

$$I_{(v,t)} = \bar{g} \cdot m \cdot h \cdot (V_{(t)} - E) \quad (4)$$

where $\bar{g}$ is the maximal conductance, m and h are activation and inactivation terms, V is the membrane potential, and E the reversal potential of the channel. The reversal potentials for $Na+$ and $K+$ were E_{Na} = 50 mV and E_K = -85 mV, respectively. The equations describing the different channel kinetics (m, h) for every current were obtained from Hemond et al. [12]. Following this reference, the three calcium conductances (T, N and L) were incorporated into a single parameter g_{Ca}.

The set of maximal conductance values that are consistent with all our experimentally observed firing patterns are shown in the Fig S1. The intracellular calcium dynamics were modeled [12], as follows:

$$\frac{\mathrm{d}[Ca^{2+}]_i}{\mathrm{d}t} = \frac{\mathrm{I}_{Ca}}{2Fv} - \frac{[Ca^{2+}]_i - 0.0001}{\tau_{Ca}} \quad (5)$$

The first term of the above equation describes the change caused by Ca^{2+} influx into a compartment with volume v. F is the Faraday constant, I_{Ca} is the calcium current and τ_{Ca} is the time constant of Ca^{2+} diffusion.

The occasional decrease in spike amplitude seen in some of the experimental traces is probably due to sodium inactivation. We choose not to include this feature in the model, because it does not affect the overall dynamics of the spike discharge itself.

3 Acknowledgments

We thank Kevan Martin for critical comments on the manuscript, Beat Gähwiler for useful discussions, and Gabriela Michel and Marion Betizeau for proofreading the manuscript.

4 Competing Interests

All authors declare that they have no competing interests.

bioRxiv preprint doi: https://doi.org/10.1101/084152; this version posted May 11, 2017. The copyright holder for this preprint (which was not certified by peer review) is the author/funder, who has granted bioRxiv a license to display the preprint in perpetuity. It is made available under aCC-BY-NC-ND 4.0 International license.

References

1. Ramon y Cajal D. Nuevo concepto de la histologia de los centros nerviosos. 1893;.
2. McCormick DA, Connors BW, Lighthall JW, Prince DA. Comparative electrophysiology of pyramidal and sparsely spiny stellate neurons of the neocortex. Journal of neurophysiology. 1985;54(4):782–806.
3. Ren J, Aika Y, Heizmann C, Kosaka T. Quantitative analysis of neurons and glial cells in the rat somatosensory cortex, with special reference to GABAergic neurons and parvalbumin-containing neurons. Experimental brain research. 1992;92(1):1–14.
4. DeFelipe J. Neocortical neuronal diversity: chemical heterogeneity revealed by colocalization studies of classic neurotransmitters, neuropeptides, calcium-binding proteins, and cell surface molecules. Cerebral Cortex. 1993;3(4):273–289.
5. Kawaguchi Y, Kubota Y. GABAergic cell subtypes and their synaptic connections in rat frontal cortex. Cerebral cortex. 1997;7(6):476–486.
6. Markram H, Toledo-Rodriguez M, Wang Y, Gupta A, Silberberg G, Wu C. Interneurons of the neocortical inhibitory system. Nature Reviews Neuroscience. 2004;5(10):793–807.
7. Somogyi P, Klausberger T. Defined types of cortical interneurone structure space and spike timing in the hippocampus. The Journal of physiology. 2005;562(1):9–26.
8. Connors BW, Gutnick MJ. Intrinsic firing patterns of diverse neocortical neurons. Trends in neurosciences. 1990;13(3):99–104.
9. Cauli B, Porter JT, Tsuzuki K, Lambolez B, Rossier J, Quenet B, et al. Classification of fusiform neocortical interneurons based on unsupervised clustering. Proceedings of the National Academy of Sciences. 2000;97(11):6144–6149.
10. Butt SJ, Fuccillo M, Nery S, Noctor S, Kriegstein A, Corbin JG, et al. The temporal and spatial origins of cortical interneurons predict their physiological subtype. Neuron. 2005;48(4):591–604.
11. Dumitriu D, Cossart R, Huang J, Yuste R. Correlation between axonal morphologies and synaptic input kinetics of interneurons from mouse visual cortex. Cerebral cortex. 2007;17(1):81–91.
12. Hemond P, Epstein D, Boley A, Migliore M, Ascoli GA, Jaffe DB. Distinct classes of pyramidal cells exhibit mutually exclusive firing patterns in hippocampal area CA3b. Hippocampus. 2008;18(4):411–424.
13. Tasic B, Menon V, Nguyen TN, Kim TK, Jarsky T, Yao Z, et al. Adult mouse cortical cell taxonomy revealed by single cell transcriptomics. Nature neuroscience. 2016;19(2):335–346.
14. Steriade M. Neocortical cell classes are flexible entities. Nature reviews neuroscience. 2004;5(2):121–134.
15. Ascoli GA, Alonso-Nanclares L, Anderson SA, Barrionuevo G, Benavides-Piccione R, Burkhalter A, et al. Petilla terminology: nomenclature of features of GABAergic interneurons of the cerebral cortex. Nature Reviews Neuroscience. 2008;9(7):557–568.

bioRxiv preprint doi: https://doi.org/10.1101/084152; this version posted May 11, 2017. The copyright holder for this preprint (which was not certified by peer review) is the author/funder, who has granted bioRxiv a license to display the preprint in perpetuity. It is made available under aCC-BY-NC-ND 4.0 International license.

16. Tricoire L, Pelkey KA, Erkkila BE, Jeffries BW, Yuan X, McBain CJ. A blueprint for the spatiotemporal origins of mouse hippocampal interneuron diversity. The Journal of Neuroscience. 2011;31(30):10948–10970.

17. Van Aerde KI, Feldmeyer D. Morphological and physiological characterization of pyramidal neuron subtypes in rat medial prefrontal cortex. Cerebral cortex. 2015;25(3):788–805.

18. Hille B. Ion channels of excitable membranes. vol. 507. Sinauer Sunderland, MA; 2001.

19. Turrigiano G, LeMasson G, Marder E. Selective regulation of current densities underlies spontaneous changes in the activity of cultured neurons. The Journal of neuroscience. 1995;15(5):3640–3652.

20. Turrigiano GG, Nelson SB. Homeostatic plasticity in the developing nervous system. Nature Reviews Neuroscience. 2004;5(2):97–107.

21. Marder E, Goaillard JM. Variability, compensation and homeostasis in neuron and network function. Nature Reviews Neuroscience. 2006;7(7):563–574.

22. Flavell SW, Greenberg ME. Signaling mechanisms linking neuronal activity to gene expression and plasticity of the nervous system. Annual review of neuroscience. 2008;31:563.

23. Cohen S, Greenberg ME. Communication between the synapse and the nucleus in neuronal development, plasticity, and disease. Annual review of cell and developmental biology. 2008;24:183–209.

24. Moody WJ, Bosma MM. Ion channel development, spontaneous activity, and activity-dependent development in nerve and muscle cells. Physiological reviews. 2005;85(3):883–941.

25. García NVDM, Karayannis T, Fishell G. Neuronal activity is required for the development of specific cortical interneuron subtypes. Nature. 2011;472(7343):351–355.

26. Dehorter N, Ciceri G, Bartolini G, Lim L, del Pino I, Marín O. Tuning of fast-spiking interneuron properties by an activity-dependent transcriptional switch. Science. 2015;349(6253):1216–1220.

27. Brandalise F, Gerber U. Mossy fiber-evoked subthreshold responses induce timing-dependent plasticity at hippocampal CA3 recurrent synapses. Proceedings of the National Academy of Sciences. 2014;111(11):4303–4308.

28. Brandalise F, Carta S, Helmchen F, Lisman J, Gerber U. Dendritic NMDA spikes are necessary for timing-dependent associative LTP in CA3 pyramidal cells. Nature Communications. 2016;7:13480.

29. Davis MJ, Wu X, Nurkiewicz TR, Kawasaki J, Gui P, Hill MA, et al. Regulation of ion channels by protein tyrosine phosphorylation. American Journal of Physiology-Heart and Circulatory Physiology. 2001;281(5):H1835–H1862.

30. Druckmann S, Hill S, Schürmann F, Markram H, Segev I. A hierarchical structure of cortical interneuron electrical diversity revealed by automated statistical analysis. Cerebral Cortex. 2013;23(12):2994–3006.

bioRxiv preprint doi: https://doi.org/10.1101/084152; this version posted May 11, 2017. The copyright holder for this preprint (which was not certified by peer review) is the author/funder, who has granted bioRxiv a license to display the preprint in perpetuity. It is made available under aCC-BY-NC-ND 4.0 International license.

31. Hosp JA, Strüber M, Yanagawa Y, Obata K, Vida I, Jonas P, et al. Morpho-physiological criteria divide dentate gyrus interneurons into classes. Hippocampus. 2014;24(2):189–203.

32. Desai NS, Rutherford LC, Turrigiano GG. Plasticity in the intrinsic excitability of cortical pyramidal neurons. Nature neuroscience. 1999;2(6):515–520.

33. Abbott LF, Nelson SB. Synaptic plasticity: taming the beast. Nature neuroscience. 2000;3:1178–1183.

34. Fan Y, Fricker D, Brager DH, Chen X, Lu HC, Chitwood RA, et al. Activity-dependent decrease of excitability in rat hippocampal neurons through increases in Ih. Nature neuroscience. 2005;8(11):1542–1551.

35. Turrigiano G, Abbott L, Marder E. Activity-dependent changes in the intrinsic properties of cultured neurons. Science-AAAS-Weekly Paper Edition-including Guide to Scientific Information. 1994;264(5161):974–976.

36. Cudmore RH, Fronzaroli-Molinieres L, Giraud P, Debanne D. Spike-time precision and network synchrony are controlled by the homeostatic regulation of the D-type potassium current. Journal of Neuroscience. 2010;30(38):12885–12895.

37. Hyun JH, Eom K, Lee KH, Ho WK, Lee SH. Activity-dependent downregulation of D-type K+ channel subunit Kv1. 2 in rat hippocampal CA3 pyramidal neurons. The Journal of physiology. 2013;591(22):5525–5540.

38. Su H, Sochivko D, Becker A, Chen J, Jiang Y, Yaari Y, et al. Upregulation of a T-type Ca2+ channel causes a long-lasting modification of neuronal firing mode after status epilepticus. The Journal of neuroscience. 2002;22(9):3645–3655.

39. Thompson L, Moyer J, Disterhoft J. Transient changes in excitability of rabbit CA3 neurons with a time course appropriate to support memory consolidation. Journal of Neurophysiology. 1996;76(3):1836–1849.

40. Gähwiler B. Organotypic monolayer cultures of nervous tissue. Journal of neuroscience methods. 1981;4(4):329–342.

41. Gähwiler B. Organotypic cultures of neural tissue. Trends in neurosciences. 1988;11(11):484–489.

42. Okamoto K, Ishikawa T, Abe R, Ishikawa D, Kobayashi C, Mizunuma M, et al. Ex vivo cultured neuronal networks emit in vivo-like spontaneous activity. The Journal of Physiological Sciences. 2014;64(6):421–431.

43. Zhang W, Linden DJ. The other side of the engram: experience-driven changes in neuronal intrinsic excitability. Nature Reviews Neuroscience. 2003;4(11):885–900.

44. McKay BM, Oh MM, Disterhoft JF. Learning increases intrinsic excitability of hippocampal interneurons. The Journal of Neuroscience. 2013;33(13):5499–5506.

45. Golowasch J, Abbott L, Marder E. Activity-dependent regulation of potassium currents in an identified neuron of the stomatogastric ganglion of the crab Cancer borealis. Journal of Neuroscience. 1999;19:RC33–1.

46. Lee PR, COHEN JE, BECKER KG, FIELDS RD. Gene Expression in the Conversion of Early-Phase to Late-Phase Long-Term Potentiation. Annals of the New York Academy of Sciences. 2005;1048(1):259–271.

bioRxiv preprint doi: https://doi.org/10.1101/084152; this version posted May 11, 2017. The copyright holder for this preprint (which was not certified by peer review) is the author/funder, who has granted bioRxiv a license to display the preprint in perpetuity. It is made available under aCC-BY-NC-ND 4.0 International license.

47. Aizenman CD, Linden DJ. Rapid, synaptically driven increases in the intrinsic excitability of cerebellar deep nuclear neurons. Nature neuroscience. 2000;3(2):109–111.

48. Jensen MS, Azouz R, Yaari Y. Variant firing patterns in rat hippocampal pyramidal cells modulated by extracellular potassium. Journal of Neurophysiology. 1994;71(3):831–839.

49. Su H, Alroy G, Kirson ED, Yaari Y. Extracellular calcium modulates persistent sodium current-dependent burst-firing in hippocampal pyramidal neurons. The Journal of Neuroscience. 2001;21(12):4173–4182.

50. Kim D, Song I, Keum S, Lee T, Jeong MJ, Kim SS, et al. Lack of the burst firing of thalamocortical relay neurons and resistance to absence seizures in mice lacking α 1G T-type Ca 2+ channels. Neuron. 2001;31(1):35–45.

51. Wu WW, Chan CS, Surmeier DJ, Disterhoft JF. Coupling of L-type Ca2+ channels to KV7/KCNQ channels creates a novel, activity-dependent, homeostatic intrinsic plasticity. Journal of neurophysiology. 2008;100(4):1897–1908.

52. Brown JT, Randall AD. Activity-dependent depression of the spike after-depolarization generates long-lasting intrinsic plasticity in hippocampal CA3 pyramidal neurons. The Journal of physiology. 2009;587(6):1265–1281.

53. Sherman SM. Tonic and burst firing: dual modes of thalamocortical relay. Trends in neurosciences. 2001;24(2):122–126.

54. Shin J, Koch C, Douglas R. Adaptive neural coding dependent on the time-varying statistics of the somatic input current. Neural computation. 1999;11(8):1893–1913.

55. Benda J, Herz AV. A universal model for spike-frequency adaptation. Neural computation. 2003;15(11):2523–2564.

56. Remme MW, Donato R, Mikiel-Hunter J, Ballestero JA, Foster S, Rinzel J, et al. Subthreshold resonance properties contribute to the efficient coding of auditory spatial cues. Proceedings of the National Academy of Sciences. 2014;111(22):E2339–E2348.

57. Hutcheon B, Yarom Y. Resonance, oscillation and the intrinsic frequency preferences of neurons. Trends in neurosciences. 2000;23(5):216–222.

58. Hu H, Vervaeke K, Storm JF. Two forms of electrical resonance at theta frequencies, generated by M-current, h-current and persistent Na+ current in rat hippocampal pyramidal cells. The Journal of physiology. 2002;545(3):783–805.

59. Schreiber S, Fellous JM, Tiesinga P, Sejnowski TJ. Influence of ionic conductances on spike timing reliability of cortical neurons for suprathreshold rhythmic inputs. Journal of neurophysiology. 2004;91(1):194–205.

60. Llinás RR. The intrinsic electrophysiological properties of mammalian neurons: insights into central nervous system function. Science. 1988;242(4886):1654–1664.

61. Buzsáki G, Draguhn A. Neuronal oscillations in cortical networks. Science. 2004;304(5679):1926–1929.

bioRxiv preprint doi: https://doi.org/10.1101/084152; this version posted May 11, 2017. The copyright holder for this preprint (which was not certified by peer review) is the author/funder, who has granted bioRxiv a license to display the preprint in perpetuity. It is made available under aCC-BY-NC-ND 4.0 International license.

62. Stemmler M, Koch C. How voltage-dependent conductances can adapt to maximize the information encoded by neuronal firing rate. Nature neuroscience. 1999;2(6):521–527.

63. Honnuraiah S, Narayanan R. A calcium-dependent plasticity rule for HCN channels maintains activity homeostasis and stable synaptic learning. PloS one. 2013;8(2):e55590.

64. Joshi P, Triesch J. Rules for information maximization in spiking neurons using intrinsic plasticity. In: Neural Networks, 2009. IJCNN 2009. International Joint Conference on. IEEE; 2009. p. 1456–1461.

65. Benna MK, Fusi S. Computational principles of synaptic memory consolidation. Nature neuroscience. 2016;.

66. Berndt DJ, Clifford J. Using Dynamic Time Warping to Find Patterns in Time Series. In: KDD workshop. vol. 10. Seattle, WA; 1994. p. 359–370.

67. Keogh E, Ratanamahatana CA. Exact indexing of dynamic time warping. Knowledge and information systems. 2005;7(3):358–386.

68. Ward Jr JH. Hierarchical grouping to optimize an objective function. Journal of the American statistical association. 1963;58(301):236–244.

69. Cooley J, Dodge F. Digital computer solutions for excitation and propagation of the nerve impulse. Biophysical journal. 1966;6(5):583–599.

70. De Schutter E, Bower JM. An active membrane model of the cerebellar Purkinje cell. I. Simulation of current clamps in slice. Journal of neurophysiology. 1994;71(1):375–400.

71. Hines ML, Carnevale NT. The NEURON simulation environment. Neural computation. 1997;9(6):1179–1209.

bioRxiv preprint doi: https://doi.org/10.1101/084152; this version posted May 11, 2017. The copyright holder for this preprint (which was not certified by peer review) is the author/funder, who has granted bioRxiv a license to display the preprint in perpetuity. It is made available under aCC-BY-NC-ND 4.0 International license.

Supporting information

bioRxiv preprint doi: https://doi.org/10.1101/084152; this version posted May 11, 2017. The copyright holder for this preprint (which was not certified by peer review) is the author/funder, who has granted bioRxiv a license to display the preprint in perpetuity. It is made available under aCC-BY-NC-ND 4.0 International license.

	Intrinsic Burst		Adapting		Accelerating		Non-Adapting		Delayed	
Maximal Conductances	Cylinder	Realistic CA3	Cylinder	Realistic CA3	Cylinder	Realistic CA3	Cylinder	Realistic CA3	Cylinder	Realistic CA3
g_{Na}	0.04	0.022	0.04	0.022	0.04	0.022	0.04	0.022	0.04	0.022
g_{Kdr}	0.01	0.01	0.01	0.01	0.01	0.02	0.01	0.01	0.02	0.01
g_{Ka}	0.07	0.02	0.04	0.02	0.04	0.02	0.12	0.02	0.08	0.02
g_{CaT}	0.001	0.00002	0.00	0.00001	0.0003	0.00001	0.00	0.00	0.0001	0.00
g_{CaN}	0.001	0.00002	0.00	0.00001	0.0003	0.00001	0.00	0.00	0.0001	0.00
g_{CaL}	0.001	0.00002	0.00	0.00001	0.0003	0.00001	0.00	0.00	0.0001	0.00
g_{CaK}	0.0001	0.00002	0.00	0.00	0.0005	0.00001	0.00	0.00	0.0006	0.00
g_{Km}	0.0006	0.021	0.00052	0.017	0.00	0.00	0.000003	0.00	0.000003	0.00
g_{Kd}	0.00045	0.002	0.00025	0.00	0.0008	0.005	0.00	0.00	0.00035	0.002
I	1	1.83	0.62	1.37	1.95	1.1	0.53	0.58	0.55	0.583

Table S1. Model maximal conductance values for the experimental fits. List of the absolute conductance values used to reproduce the traces of main Fig 4 (Intrinsic Burst, Adapting, Accelerating, Non-Adapting and Delayed) in the single compartment NEURON model. The same class of firing pattern traces could be also reproduced (second column for each trace) using the realistic CA3 pyramidal neuron model from Hemond et al. [12]. The conductances were tuned manually in order to fit qualitatively the overall dynamics of the voltage experimental traces. The bottom row lists the value of the current (in nA) used to generate every voltage trace. For more detailed description of the model see Methods.

bioRxiv preprint doi: https://doi.org/10.1101/084152; this version posted May 11, 2017. The copyright holder for this preprint (which was not certified by peer review) is the author/funder, who has granted bioRxiv a license to display the preprint in perpetuity. It is made available under aCC-BY-NC-ND 4.0 International license.

Conductances Ranges	1	2	3
g_{Kdr}	0.015 : 0.05 : 0.04		
g_{Ka}	0.01 : 0.01 : 0.09		
g_{Ca}	0	0.2 : 0.1 : 0.6	0.8 : 0.1 : 1
g_{CaK}	0 : 0.1 : 0.9		
g_{Km}	0	0.4 : 0.1 : 1	
g_{Kd}	0 : 0.1 : 0.3	0.4 : 0.05 : 0.8	0.9 : 0.1 : 1
I	0.45 : 0.05 : 0.65	0.75 : 0.05 : 1	1.75 : 0.05 : 1.95
Total conductance vectors	861		
Total traces	5166		

Table S2. Range of maximal conductance values used to generate the model database of voltage traces. A model database of voltage traces, which includes all the observed experimental firing patterns, was generated by varying 6 maximal conductances ($gKdr$, gKa , gCa , $gCaK$, gKm and gKd) over a given range. Each row in the table lists the ranges of conductance values employed in every channel. The different ranges of conductances (columns) were produced in order to account for the different firing patterns reproduced in the model. Different ranges of current were also needed to reveal the different firing types. A total of 861 conductance vectors were generated by combining the different conductances. The firing pattern of every conductance vector was produced at several levels of step-current injection, obtaining a total of 5166 voltage traces. Note that $gCaT$, $gCaN$ and $gCaL$ are englobed under the single parameter gCa.

bioRxiv preprint doi: https://doi.org/10.1101/084152; this version posted May 11, 2017. The copyright holder for this preprint (which was not certified by peer review) is the author/funder, who has granted bioRxiv a license to display the preprint in perpetuity. It is made available under aCC-BY-NC-ND 4.0 International license.

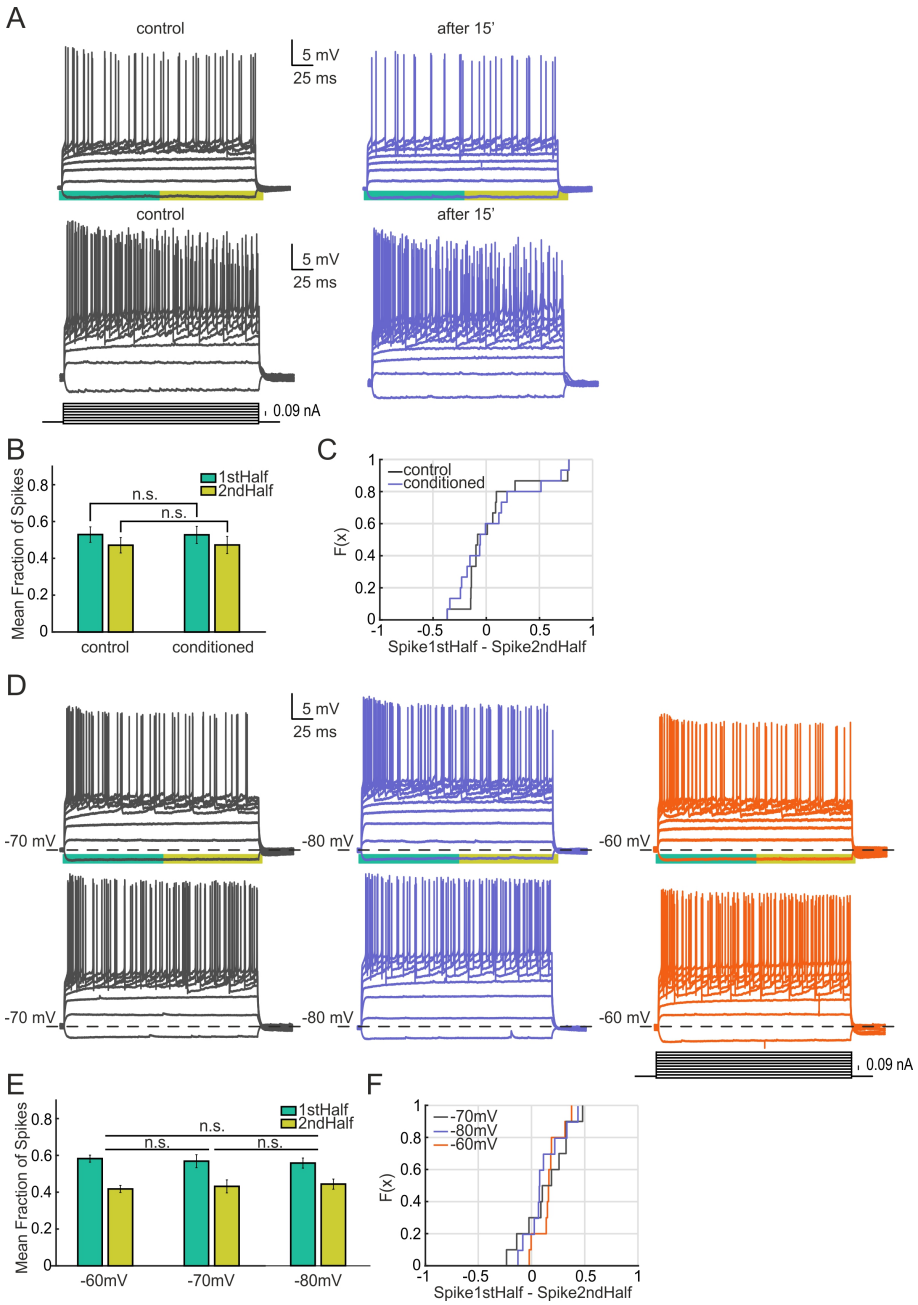

Fig S1. Stability controls. Firing pattern transitions are not elicited by step current injection alone. A) Examples of two cells whose firing pattern have been measured by step-wise current injection (protocol showed in the inset). The cells do not show changes in firing pattern after 15 min of recording. B) Mean Fraction of Spikes for the population in the first and second half of the voltage trace for both control and conditioned cases. No significant redistribution on the fraction of spikes is observed (n = 15, p=0.583, two-sided Wilcoxon signed rank test). C) Empirical Cumulative Distribution Function for the data shown in B. Every individual case is represented as the number of spikes for the first half of the trace minus the spikes for the second half. D) Firing pattern transitions are not elicited by sustained shifts in membrane potential. Examples of two cells that have been hold at different membrane potentials through steady current injection (-70, -80 and -60 approximately). After changing the holding potential of the recorded neuron the firing patter was measured by step-wise current injection (protocol showed in the inset). No transitions of firing pattern were observed at any of the different holding potentials. E) Mean Fraction of Spikes for the population in the first and second half of the voltage trace for every condition. No significant redistribution on the fraction of spikes is observed (Vm 60 vs 70, p=0.652; Vm 60 vs 80, p=0.084; Vm 70 vs 80, p=0.695) (n = 10, two-sided Wilcoxon signed rank test)). F) Empirical Cumulative Distribution Function for the data shown in E. Every individual case is represented as the number of spikes for the first half of the trace minus the spikes for the second half.

bioRxiv preprint doi: https://doi.org/10.1101/084152; this version posted May 11, 2017. The copyright holder for this preprint (which was not certified by peer review) is the author/funder, who has granted bioRxiv a license to display the preprint in perpetuity. It is made available under aCC-BY-NC-ND 4.0 International license.

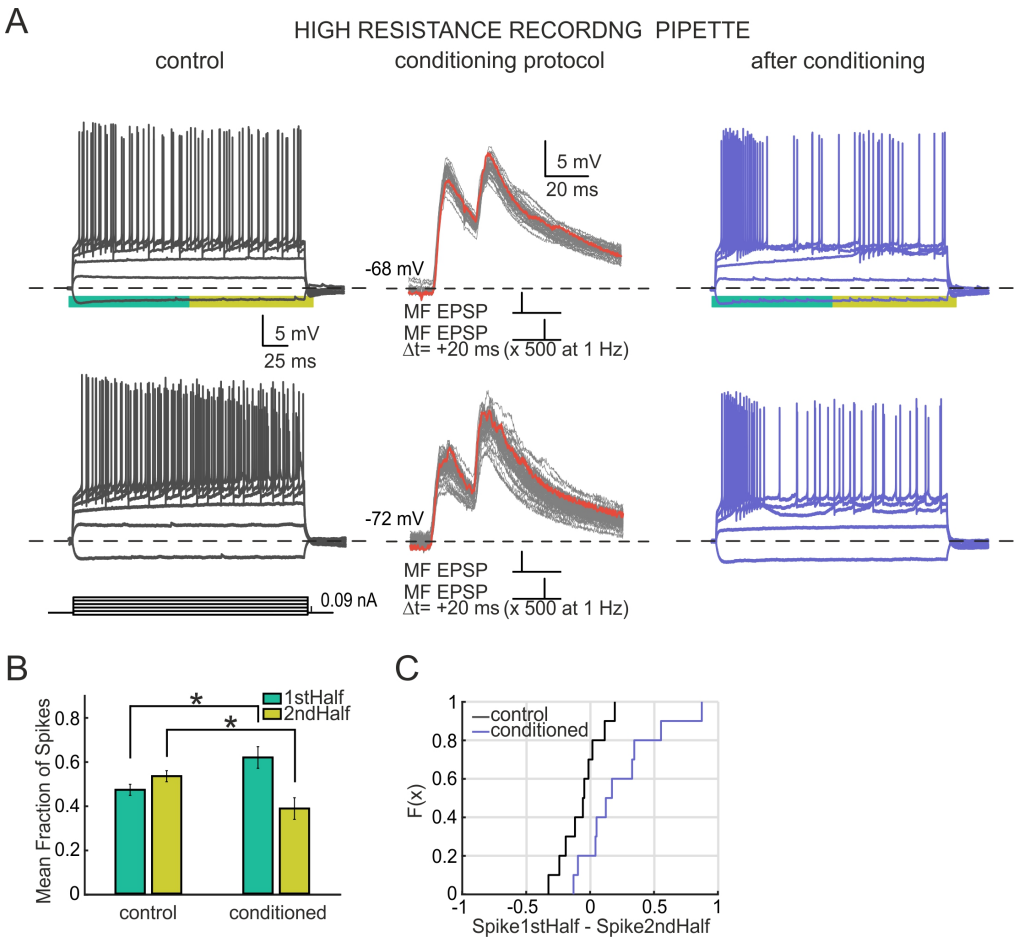

Fig S2. Firing pattern transitions on CA3 neurons are not induced by intracellular dialysis. A) Two cells patched with high resistance pipettes (10MΩ). Two sample control cells that exhibit non-adapting (upper panel) and accelerating (lower panel) firing pattern. After conditioning, both change to intrinsic burst firing pattern. The mossy fiber stimulation protocol is shown in middle panel. B) Mean Fraction of Spikes for the population in the first and second half of the voltage trace for both control and conditioned cases. A significant redistribution on the fraction of spikes is observed after the conditioning, where the fraction of spikes on the first half is increased while it decreases in the second half (n=10, p=0.048, two-sided Wilcoxon signed rank test). C) Empirical Cumulative Distribution Function for the data shown in B. Every individual case is represented as the number of spikes for the first half of the trace minus the spikes for the second half.

bioRxiv preprint doi: https://doi.org/10.1101/084152; this version posted May 11, 2017. The copyright holder for this preprint (which was not certified by peer review) is the author/funder, who has granted bioRxiv a license to display the preprint in perpetuity. It is made available under aCC-BY-NC-ND 4.0 International license.

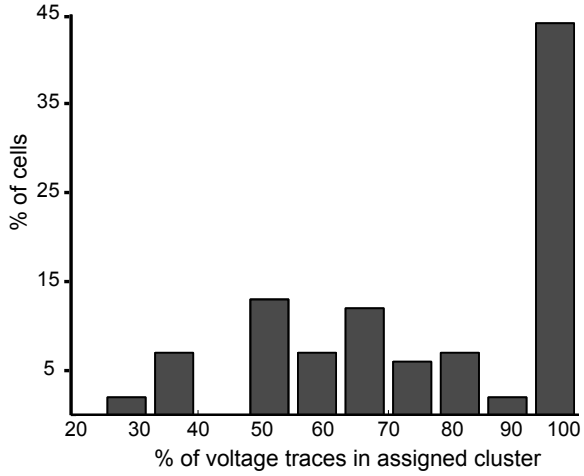

Fig S3. Clustering performance on the step-wise voltage traces. The capacity of the clustering algorithm to group together independent voltage traces derived from the same set of current injections was evaluated. Histogram x-axis accounts for the percentage of voltage traces from the same set that are assigned to a unique cluster. Y-axis, shows the percentage of cells that fulfill the x condition. Ideal performance of the algorithm would allocates 100% of voltage traces coming from same set of current injections to the same cluster. For most of the cells, at least half of the voltage traces fall into one cluster, and almost 45% of the cells have all traces (100%) assigned to same cluster (n=50).

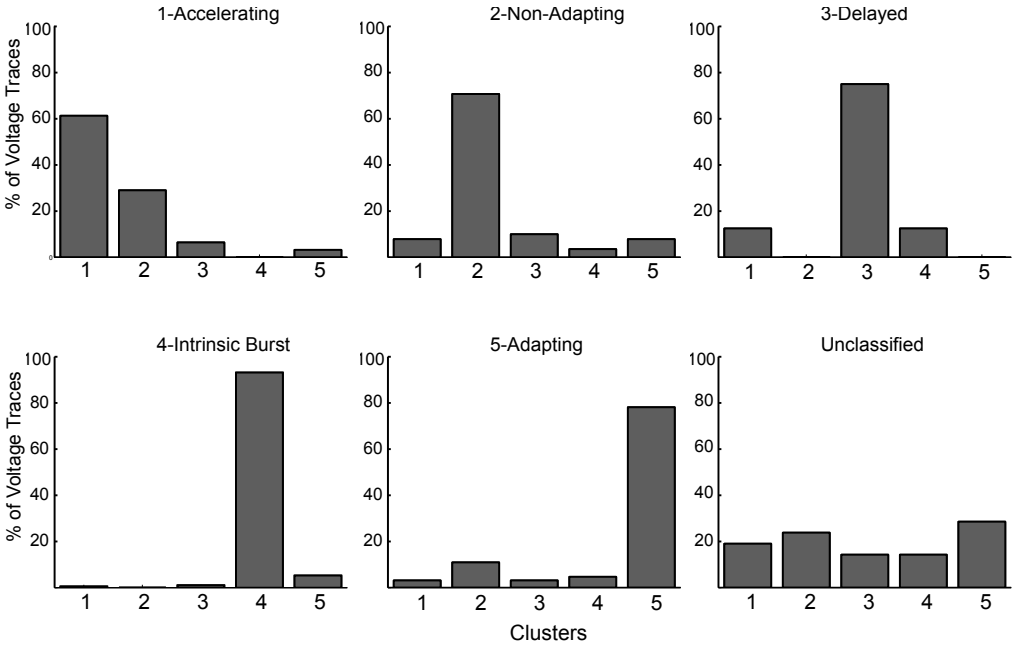

Fig S4. Misclassified voltage traces from an assigned cell. Each panel shows the percentage of voltage traces of the cells assigned to a given cluster, which have been assigned by the algorithm to the other clusters. For example, first panel shows that 30% of voltage traces of cells classified as Accelerating fall into the Non-Adapting cluster. At higher current injection the accelerating pattern is lost. Because of high firing rate the algorithm now classifies the traces as non-adapting . Numbers on the x axis correspond to the different cluster classes. 1-Accelerating, 2-Non-Adapting, 3-Delayed, 4-Intrinsic Burst, 5-Adapting. Last panel shows the distribution of voltage traces of unclassified cells. (n=50)

bioRxiv preprint doi: https://doi.org/10.1101/084152; this version posted May 11, 2017. The copyright holder for this preprint (which was not certified by peer review) is the author/funder, who has granted bioRxiv a license to display the preprint in perpetuity. It is made available under aCC-BY-NC-ND 4.0 International license.

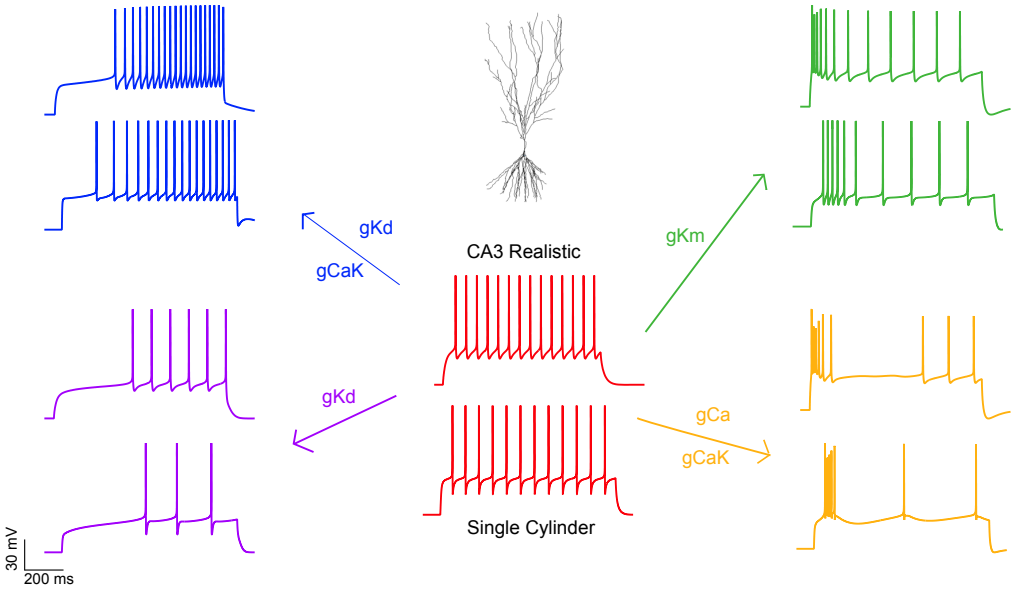

Fig S5. Firing pattern transitions can be reproduced in both, a single compartment model and a realistic CA3 pyramidal model. We find that the key ion channels responsible of the firing pattern transitions are kept in both the single compartment model and the realistic one. The upper trace represents the model traces reproduced on the CA3 realistic pyramidal cell, and below the same firing pattern on the single cylinder is shown. The maximal conductance values used to reproduce every pattern are shown in the Table S2.

bioRxiv preprint doi: https://doi.org/10.1101/084152; this version posted May 11, 2017. The copyright holder for this preprint (which was not certified by peer review) is the author/funder, who has granted bioRxiv a license to display the preprint in perpetuity. It is made available under aCC-BY-NC-ND 4.0 International license.

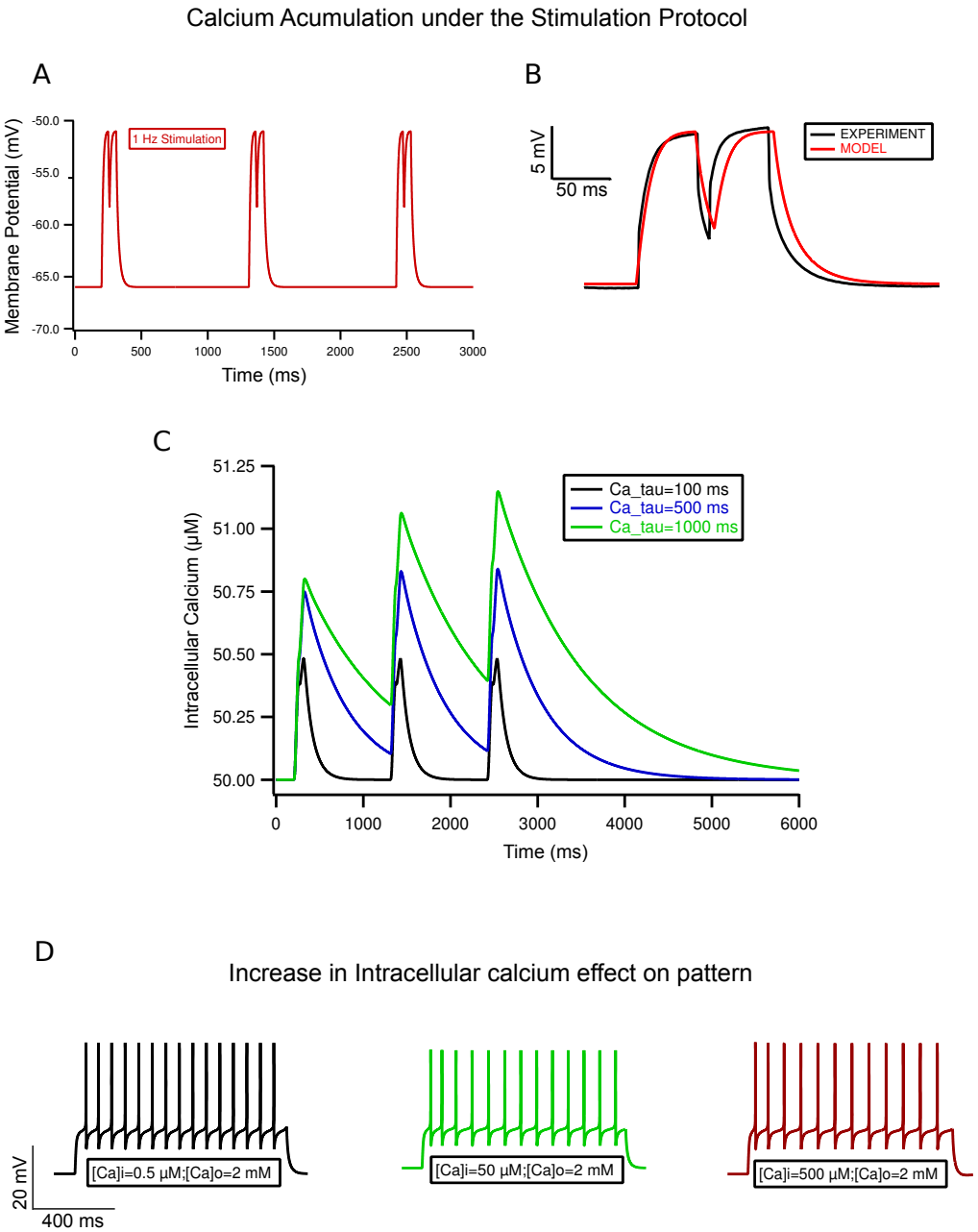

Fig S6. Firing pattern transitions in the model are not due to calcium accumulation. A) Protocol applied to the model cell: 1 Hz current stimulation by double current pulses that elicited a depolarization of 10 mV, repeated 500 times. B) Comparison of model pulses with those elicited in the soma of experimental cells. C) Due to kinetics of calcium decay, the ion does not accumulate over period of stimulation (black trace). Decay must be much longer for calcium to accumulate significantly (green trace). D) Hypothetical increase in intracellular increase has little effect on pattern of discharge, even when increased 1000 fold (from left to right).

bioRxiv preprint doi: https://doi.org/10.1101/084152; this version posted May 11, 2017. The copyright holder for this preprint (which was not certified by peer review) is the author/funder, who has granted bioRxiv a license to display the preprint in perpetuity. It is made available under aCC-BY-NC-ND 4.0 International license.

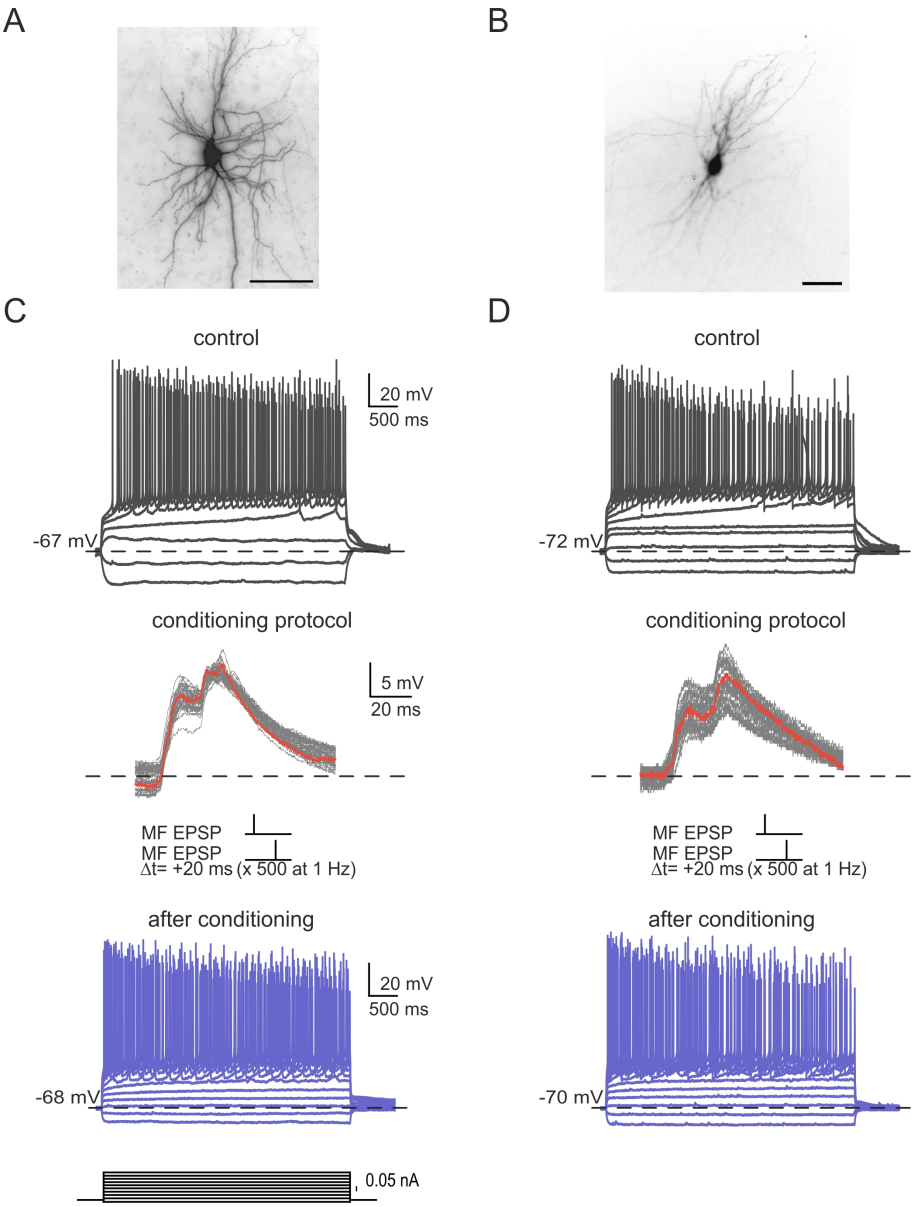

Fig S7. Selected cells with high frequency firing do not switch to adapting or intrinsic burst firings. A) Biocytin filled spiny cell with stellate morphology. B) Smooth cell with rounded somata and short dense dendritic arbor. Firing patterns in control (upper) and after stimulation (bottom) are shown beneath each cell for both the stellate (C) and the smooth cell (D). The neurons present a non-adapting pattern both, before and after conditioning. Middle panel shows EPSPs elicited in the cell via mossy fiber stimulation. Note that after conditioning, cells do not change the generic Petilla firing pattern mode (Fast Spiking), although there is a visible modulation on the delay to first spike ('ramping response'). Scale bar = 50μm